

International Journal of Modern Physics E
 © World Scientific Publishing Company

COUPLING OF SURFACE AND VOLUME DIPOLE OSCILLATIONS IN C₆₀ MOLECULES

M. BRACK

*Institute of Theoretical Physics, University of Regensburg, D-93040 Regensburg, Germany
 e-mail: matthias.brack@physik.uni-regensburg.de*

P. WINKLER

Department of Physics, University of Nevada Reno, NV 89557, USA

M. V. N. MURTHY

Institute of Mathematical Sciences, CIT Campus, Taramani, Chennai 600 113, India

Received (August 29, 2021)

Revised (revised date)

We first give a short review of the “local-current approximation” (LCA), derived from a general variation principle, which serves as a semiclassical description of strongly collective excitations in finite fermion systems starting from their quantum-mechanical mean-field ground state. We illustrate it for the example of coupled translational and compressional dipole excitations in metal clusters. We then discuss collective electronic dipole excitations in C₆₀ molecules (Buckminster fullerenes). We show that the coupling of the pure translational mode (“surface plasmon”) with compressional volume modes in the semiclassical LCA yields semi-quantitative agreement with microscopic time-dependent density functional (TDLDA) calculations, while both theories yield qualitative agreement with the recent experimental observation of a “volume plasmon”.

1. Introduction

Early in the history of nuclear physics, the (isovector) giant dipole resonance (GDR) provided one of the first manifestations of strongly collective excitations in finite fermion systems. Two classical models were suggested to describe the physics of the GDR: a) the model of Goldhaber and Teller,¹ in which protons and neutrons are both incompressible fluids undergoing a relative translational oscillation, and b) the model of Steinwedel and Jensen² (previously also proposed by Migdal³), in which protons and neutrons are both locally decompressed or compressed with opposite phases, such that the total nuclear density remains constant and a dipole oscillation results (cf. Fig. 1 below). Detailed analysis of experimental data revealed later that a suitable combination of both models was necessary to interpret these data,^{4,5} so that the GDR could be classically best understood in terms of coupled translational and compressional dipole modes. These early classical models were

later refined by the so-called “fluid dynamics”⁶ and the “sum rule approach”⁷ based on the selfconsistent mean-field description of collective excitations in the random phase approximation (RPA).⁸ These semiclassical models were successfully used to describe collective excitations not only in nuclei, but also in metal clusters,^{9,11,10} where a similar coupling between translational and compressional dipole modes has been shown to well describe the collective optical response.^{12,13,14}

In this paper, we review the “local current approximation” (LCA), which encompasses both the fluid-dynamical and sum rule approaches and can be derived from a variational principle on the same footing as the RPA, and quote some of its results for metal clusters. We then apply the LCA to collective electronic excitations in C₆₀ molecules, for which recent experiments¹⁵ have revealed a “volume plasmon”, a broad high-energy shoulder in the photo-ionization cross section (otherwise dominated by the “surface plasmon”^{16,17}) which again can be semiclassically understood as a compressional component of the collective dipole excitation.

2. The local current approximation (LCA)

The stationary Schrödinger equation $\hat{H}|\nu\rangle = (\hat{T} + \hat{V})|\nu\rangle = E_\nu|\nu\rangle$ for a many-body system can be cast into the following well-known “equations of motion”:⁸

$$\begin{aligned} \langle 0|\mathcal{O}_\nu[\hat{H}, \mathcal{O}_\nu^\dagger]|0\rangle &= \hbar\omega_\nu\langle 0|\mathcal{O}_\nu\mathcal{O}_\nu^\dagger|0\rangle, \\ \langle 0|\mathcal{O}_\nu[\hat{H}, \mathcal{O}_\nu]|0\rangle &= \hbar\omega_\nu\langle 0|\mathcal{O}_\nu\mathcal{O}_\nu|0\rangle = 0, \end{aligned} \quad (1)$$

where the operators \mathcal{O}_ν^\dagger and \mathcal{O}_ν are defined by

$$\mathcal{O}_\nu^\dagger|0\rangle = |\nu\rangle, \quad \mathcal{O}_\nu|\nu\rangle = |0\rangle, \quad \mathcal{O}_\nu|0\rangle = 0. \quad (2)$$

$|0\rangle$ is the ground state and $\hbar\omega_\nu = E_\nu - E_0$ ($\nu > 0$) are the excitation energies. As shown in Ref.¹⁸, Eq. (1) can be rederived by the following variational principle:

$$\delta E_3[\hat{Q}]/\delta\hat{Q} = 0, \quad E_3[\hat{Q}] := \sqrt{m_3[\hat{Q}]/m_1[\hat{Q}]}, \quad (3)$$

where the “moments” m_1 and m_3 – cf. (15) for their names – are defined by

$$m_1[\hat{Q}] := \frac{1}{2}\langle 0|[\hat{Q}, [\hat{H}, \hat{Q}]]|0\rangle, \quad m_3[\hat{Q}] := \frac{1}{2}\langle 0|[[\hat{H}, \hat{Q}], [[\hat{H}, \hat{Q}], \hat{H}]]|0\rangle. \quad (4)$$

As long as \hat{Q} is taken to be the most general (nonlocal) hermitean operator, the system (3,4) is equivalent to the exact stationary Schrödinger equation. Successive orthogonalization of $\hat{Q}_1, \hat{Q}_2, \dots$ yields the exact excitation spectrum $E_3(\hat{Q}_\nu) = \hbar\omega_\nu$ ($\nu = 1, 2, \dots$). With $\hat{Q}_\nu \propto \mathcal{O}_\nu^\dagger + \mathcal{O}_\nu$, which may be interpreted as a set of generalized coordinates (cf. Refs.^{8,13}), we are brought back to (1).

In the selfconsistent microscopic mean-field approaches, one replaces $|0\rangle$ either by a Slater determinant (Hartree-Fock theory, HF) or by the Kohn-Sham (KS) ground state in terms of the local density $\rho(\mathbf{r})$ (density functional theory, DFT). If the operator \hat{Q} in (4) is replaced by a one-particle-one-hole ($1p1h$) operator, its variation (3) leads to the RPA equations. [The RPA ground state should in principle

contain $2p2h$ excitations, but due to a theorem by Thouless¹⁹ one may use the HF ground state for computing $m_1[Q_\nu]$ and $m_3[Q_\nu]$ in (4).] In the framework of DFT (using the local density approximation, LDA, for the exchange-correlation energy), the RPA is often also referred to as the time-dependent LDA (TDLDA).

In the sum rule and fluid dynamical approaches, one approximates the collective excitation energies $\hbar\omega_\nu$ by the energy $E_3[Q_\nu]$, defined as in (3,4) but in terms of suitable local model operators $Q_\nu(\mathbf{r})$, such as $Q_d = z$ to describe pure translations (Goldhaber-Teller model), the monopole operator $Q_0 = r^2$ for radial compressions (“breathing mode”); $Q_2 = r^2 Y_{20}$ for quadrupole oscillations, etc.

The **local current approximation (LCA)** consists in the following assumptions. One uses for $|0\rangle$ in (4) the uncorrelated HF or KS ground state, like in RPA or TDLDA, and takes the operator \hat{Q} in (3,4) to be a **local** function $Q(\mathbf{r})$. For local and spin-less (e.g. Coulomb) two-body interactions \hat{V} , one then obtains

$$m_1[Q] = m_1[\mathbf{u}] = \frac{m}{2\hbar^2} \int \mathbf{u}(\mathbf{r}) \cdot \mathbf{u}(\mathbf{r}) \rho(\mathbf{r}) d^3r, \quad \mathbf{u}(\mathbf{r}) = -\frac{\hbar^2}{m} \nabla Q(\mathbf{r}), \quad (5)$$

where $\mathbf{u}(\mathbf{r})$ is a local displacement field which is proportional to the collective current, see (12) below. (This justifies the name of LCA.) Note that if $\nabla^2 Q(\mathbf{r})$ and hence $\nabla \cdot \mathbf{u}(\mathbf{r})$ is zero, then one has incompressible collective flow; otherwise the collective motion involves local compression of the fermi fluid.

The moment $m_3[Q]$ is a more complicated functional of $\mathbf{u}(\mathbf{r})$, of the spatial density $\rho(\mathbf{r}) = \sum_{i=1}^N |\phi_i(\mathbf{r})|^2$ and the kinetic energy density $\tau(\mathbf{r}) = \sum_{i=1}^N |\nabla \phi_i(\mathbf{r})|^2$ (and possibly a current density according to the “current-DFT”²⁰) in terms of the ground-state HF (or KS) wave functions $\phi_i(\mathbf{r})$. The variation $\delta E_3[Q]/\delta Q(\mathbf{r}) = 0$ leads to fluid dynamical eigenvalue equations:¹⁸

$$\frac{\delta m_3[\mathbf{u}]}{\delta u_j(\mathbf{r})} = (\hbar\omega_\nu)^2 \frac{m}{\hbar^2} \rho(\mathbf{r}) u_j(\mathbf{r}) \quad (j = x, y, z) \quad (6)$$

yielding the spectrum $\hbar\omega_\nu$ and eigenmodes $\mathbf{u}_\nu(\mathbf{r})$. Eq. (6) represents three coupled nonlinear fourth-order partial differential equations for $u_j(\mathbf{r})$, which in general are extremely hard to solve. Because of their dependence on the wave functions ϕ_i , one also speaks of “quantum fluid dynamics” which includes the effects of zero sound.⁶

A practical way (“finite-basis LCA”) to solve (6) approximately consists in expanding the operator $Q(\mathbf{r})$ in a finite set of basis functions $\{Q_p(\mathbf{r})\}$:

$$Q(\mathbf{r}) = \sum_{p=1}^M c_p Q_p(\mathbf{r}). \quad (7)$$

The variational principle (3,4) then yields a set of M secular equations, whose characteristic equation is:

$$\det|C_{pp'} - (\hbar\omega_\nu)^2 B_{pp'}| = 0, \quad (p, p', \nu = 1, 2, \dots, M) \quad (8)$$

with

$$B_{pp'} = \langle 0 | [Q_p, [H, Q_{p'}]] | 0 \rangle,$$

4 *Brack, Winkler and Murthy*

$$C_{pp'} = \langle 0 | [[H, Q_p], [[H, Q_{p'}], H]] | 0 \rangle. \quad (9)$$

Solution of (8) yields the excitation energies $\hbar\omega_\nu$ and the operators $Q_\nu(\mathbf{r})$ creating the collective states $|\nu\rangle$. The characteristic equation (8) is the basic equation of the LCA and looks similar to one version of the RPA equations. The basis set $\{Q_p(\mathbf{r})\}$ must be suitably chosen; here a good physical intuition for the considered collective motion is of great help.

In a further approximation, one may replace the HF or KS ground-state density by a selfconsistent semiclassical (extended) Thomas-Fermi (ETF)²¹ type smooth density, and use the ETF functional $\tau_{ETF}[\rho]$ (and possibly a corresponding functional for the current density) in computing the ingredients of (9). Although this approximation misses the quantum shell oscillations in the densities, it has proven to be sufficient for the evaluation of collective excitation spectra in many cases.^{5,12,13,22}

The LCA is equivalent to the “generalized scaling model”,⁷ representing the system by a collective Hamiltonian

$$H_{coll} = \frac{1}{2} \sum_{p,p'=1}^M (B_{pp'} \dot{\alpha}_p \dot{\alpha}_{p'} + C_{pp'} \alpha_p \alpha_{p'}) \quad (10)$$

that describes coupled harmonic oscillations with the velocity fields $\mathbf{v}_p(\mathbf{r}, t)$:

$$\mathbf{v}_p(\mathbf{r}, t) = \dot{\alpha}_p(t) \mathbf{u}_p(\mathbf{r}) \quad (11)$$

and the **local currents**

$$\mathbf{j}_\alpha(\mathbf{r}, t) = \rho_\alpha(\mathbf{r}, t) \mathbf{v}_\alpha(\mathbf{r}, t), \quad (12)$$

which obey the continuity equation:

$$\frac{\partial}{\partial t} \rho_\alpha(\mathbf{r}, t) + \nabla \cdot \mathbf{j}_\alpha(\mathbf{r}, t) = 0. \quad (13)$$

Here $\rho_\alpha(\mathbf{r}, t)$ are the “scaled” time-dependent densities (see Refs.^{7,13,18} for their definition).

Having solved either (8) or (10), one knows the eigenmodes of the system and can calculate its response to an external excitation operator \mathbf{Q}_{ext} . To this purpose one defines a strength function:

$$S_{\mathbf{Q}_{ext}}(E) = \sum_{\nu>0} |\langle \nu | \mathbf{Q}_{ext} | 0 \rangle|^2 \delta(E - \hbar\omega_\nu), \quad (14)$$

whose energy-weighted moments $m_k(\mathbf{Q}_{ext})$ become:

$$m_k(\mathbf{Q}_{ext}) = \int_0^\infty E^k S_{\mathbf{Q}_{ext}}(E) dE = \sum_{\nu>0} (\hbar\omega_\nu)^k |\langle \nu | \mathbf{Q}_{ext} | 0 \rangle|^2. \quad (15)$$

The photo-absorption cross section $\sigma(\omega)$ in the long-wavelength limit becomes

$$\sigma(\omega) = (4\pi\omega/3c) S_{dip}(E = \hbar\omega), \quad (16)$$

where $\mathbf{Q}_{ext} = Q_{dip} = ez$ is the electric dipole operator and ω is the frequency of the external electric field.

For applications in metal clusters, the following basis set of local operators¹² has successfully been used:

$$Q_p(\mathbf{r}) = e r^p Y_{L0}(\theta). \quad (p = 1, 2, \dots, M) \quad (17)$$

We consider here only dipole modes ($L = 1$); for $p = 1$ we then have the electric dipole operator $Q_1 = Q_{dip} = ez$, while for $p > 1$ we obtain compressional dipole modes with $\nabla^2 Q_p \neq 0$. Hence, a finite set with $M \geq 2$ of these operators will allow for the description of coupled translational and vibrational dipole modes. (Alternative basis sets involve spherical Bessel functions.¹³)

It is illustrative to consider the mechanism of this coupling for the classical limit of a metal cluster in the spherical jellium model.^{11,10,23} Here the ionic density is taken to be a spherical uniform charge distribution with radius R :

$$\rho_I(r) = e\rho_0 \Theta(R - r), \quad (18)$$

where the bulk density ρ_0 is chosen such that the integrated total ionic charge is opposite to that of the valence electrons. In the classical macroscopic limit ($N \rightarrow \infty$), we take the electron charge to be opposite to that of the jellium sphere: $\rho_e(r) = -\rho_I(r)$ and neglect the kinetic and exchange-correlation contribution to the total energy, so that the system is entirely described by the dominating classical Coulomb forces. On the left side of Fig. 1, we illustrate the pure translational vibration of the electrons against the ions, described by the single dipole operator $Q_{dip} = ez$. It

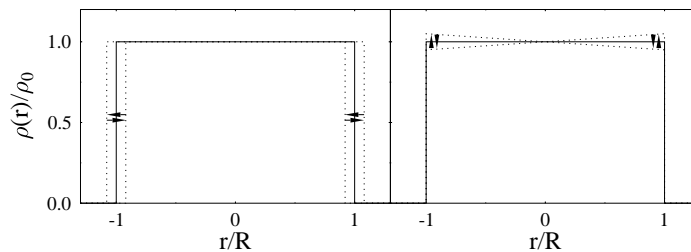


Fig. 1. Schematic picture of collective oscillations of electrons (dotted lines) against ions (solid lines) in the spherical jellium model for a metal cluster. *Left*: pure translation, yielding the Mie “surface plasmon” (cf. the Goldhaber-Teller mode in the nuclear GDR). *Right*: compressional dipole mode, leading to a “volume plasmon” (cf. the Steinwedel-Jensen-Migdal mode in nuclei).

leads to the so-called “Mie plasmon” or “surface plasmon” with the energy

$$E_3(Q_d) = \hbar\omega_{Mie} = \sqrt{\hbar^2 e^2 N / m R^3}, \quad (19)$$

where N is the number of single-valenced (e.g. sodium) atoms. This is what corresponds to the Goldhaber-Teller model for the nuclear isovector GDR. On the right

6 *Brack, Winkler and Murthy*

side of Fig. 1 we sketch a compressional mode brought about by a suitable combination of operators (17) with $p > 1$, which corresponds to the Steinwedel-Jensen (Migdal) mode for the nuclear GDR.

As shown in Ref.¹², the equation (8) can be solved analytically in the above purely Coulombic classical limit, with the following interesting solution:

When $M > 1$ modes are coupled, one of which has $p = 1$ (pure dipole mode) and all others have $M - 1$ different, but arbitrary real values $p > 1$, the spectrum always consists of one surface plasmon with frequency $\omega = \omega_{Mie}$ and $M - 1$ degenerate volume plasmons with the frequency $\omega = \omega_{vol}$.

This result could only be obtained in Ref.¹² for specific examples. A mathematical proof, for the general case of operators (17) with arbitrary L , is given in the appendix of this article.

The frequency ω_{vol} is the bulk plasma frequency ω_{pl} of the corresponding metal

$$\omega_{vol} = \omega_{pl} = \sqrt{3e^2/mr_s^3}, \quad (20)$$

r_s being its Wigner-Seitz radius. This “volume plasmon” can also be brought about as a pure compressional mode by the radial (monopole) operator $Q_0 = er^2$ (which is also used to describe the nuclear breathing mode):

$$E_3(Q_0) = \hbar\omega_{vol} = \sqrt{3\hbar^2e^2N/mR^3} = \sqrt{3}\hbar\omega_{Mie}. \quad (21)$$

This mode can, however, not be excited by the external dipole operator because it corresponds to $L = 0$, and therefore does not couple to the electric dipole field. The surface plasmon with frequency ω_{Mie} then carries all of the dipole strength.

In finite clusters with realistic smooth electronic densities $\rho_e(r)$, and including the quantum-mechanical kinetic zero-point and exchange-correlation energies, the operators (17) with $p > 1$ can couple to the electric dipole field, the degeneracy of the $M - 1$ volume plasmons is broken and their eigenmodes carry a finite amount of dipole strength.¹² Experimentally, this manifests itself in a broad shoulder, or sometimes a small extra peak, of the dipole absorption cross section, located somewhat below the energy of the bulk plasmon (21). This volume plasmon had already been anticipated in the early TDLDA calculations of Ekardt.²³

In Fig. 2 we illustrate the above with some results for singly-ionized sodium clusters (left side: Na_{27}^+ , right side: Na_{41}^+). The dots in the upper left part on each side give the experimental photo-absorption cross section.²⁴ The lower left parts give the LCA results,¹⁴ the vertical sticks correspond to the eigenvalues $\hbar\omega_\nu$ weighted by their percentage of the total dipole sum rule, and the solid curve is obtained by convoluting them with a Lorentzian to simulate continuum effects (as is customary also in discrete RPA and TDLDA calculations). On the lower right on each side we see the ionic structure,¹⁴ as obtained in Car-Parrinello type molecular calculations in the cylindrically averaged pseudopotential scheme (CAPS).²⁵ We see that the cross section of Na_{27}^+ , with a non-magic number $N = 26$ of valence electrons, clearly exhibits two main peaks which are due to the large average deformation of the ionic structure (as well-known also for the GDR in deformed nuclei). This deformation

is prolate, and hence the higher peak has roughly twice the strength of the lower peak. These two peaks here are both translational surface plasmons, split by the average deformation of the system. The volume plasmon is hardly recognizable in this case. The cluster Na_{41}^+ has a magic number^{11,26} $N=40$ of valence electrons and therefore a nearly spherical electron cloud (in spite of the non-sphericity of the ionic structure). Here the response is dominated by one relatively sharp surface peak and exhibits a plateau in the high-energy shoulder which can be identified as a volume plasmon, in fair agreement with the LCA prediction.

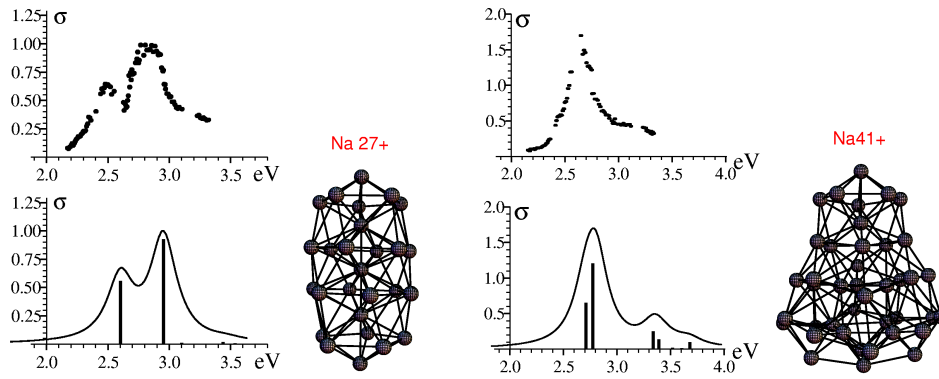
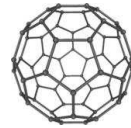


Fig. 2. Optic dipole response of Na_{27}^+ (left part) and Na_{41}^+ (right part). *Upper left*: Experimental result.²⁴ *Lower left*: LCA result.¹⁴ *Lower right*: Ionic structure from CAPS calculation.^{14,25}

3. Coupling of surface and volume modes in C_{60} molecules

We now turn to the optic response of C_{60} molecules, the famous Buckminsterfullerenes. They consist of 60 carbon atoms, each providing four valence electrons, so that $N=240$ electrons can oscillate collectively against the ionic structure. Indeed, a giant resonance peak has been predicted¹⁶ and experimentally observed¹⁷ around 20 - 22 eV, and in the framework of the jellium model²⁷ been interpreted as a Mie surface plasmon.



More recent experiments¹⁵ on the optic response of C_{60} molecules have focused at higher energies, and a broad shoulder was observed around 30 - 45 eV (see the circles in Fig. 3) which was interpreted as a volume plasmon. A two-Lorentzian fit to the single photoionization cross section positioned the surface plasmon at 22 ± 0.1 eV and the volume plasmon at 38 ± 2 eV. A TDLDA calculation^{15,28} using a readjusted version of the jellium model²⁷ yielded, besides the main surface peak at 22 eV, an extra peak around 42 eV (see the solid line in Fig. 3), without however revealing the precise nature of the corresponding collective motion. In an ensuing debate, the interpretation of the volume peak as a compressional component of the collective motion was challenged,²⁹ and defended³⁰ with reference to the well-known situation in metal clusters.

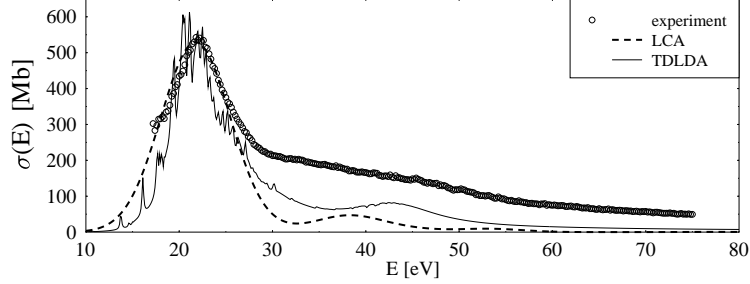
8 *Brack, Winkler and Murthy*


Fig. 3. Optic response of C_{60} molecules. *Circles*: Experimental photoionization cross section.¹⁵ *Solid lines*: TDLDA calculation^{15,28} and *dashed lines*: present LCA calculation (see text for details) of the optic dipole response. Both theoretical curves have been blue shifted by 5.5 eV and scaled to the height of the experimental surface peak.

We shall presently corroborate this interpretation in the LCA. We use the same jellium model as in the TDLDA calculation,¹⁵ in which the ionic distribution of the C_{60} molecule is replaced by a spherical shell with radius R and thickness Δ :

$$\rho_I(r) = \rho_0[\Theta(R_2 - r) - \Theta(r - R_1)], \quad (22)$$

with $R_1 = R - \Delta/2$, $R_2 = R + \Delta/2$ using the constants $R = 0.354$ nm and $\Delta = 0.153$ nm; ρ_0 is chosen such that the integrated ionic charge is opposite to that of the valence electrons.

To obtain a first rough estimate of the results to be expected, we use the same schematic classical model with $\rho_e(r) = -\rho_I(r)$ and neglecting kinetic and xc energies, as discussed above. Furthermore we keep only the leading terms in Δ/R (although this is not really a small parameter). The energy $E_3(Q)$ with the dipole operator $Q_d = ez$ then yields a Mie surface plasmon at

$$E_3(Q_d) = \hbar\omega_{Mie} = \sqrt{\hbar^2 N e^2 / 3mR^2\Delta} = 21.4 \text{ eV}, \quad (23)$$

while the monopole operator $Q_0 = er^2$ yields a volume plasmon at

$$E_3(Q_0) = \hbar\omega_{vol} = \sqrt{3} \hbar\omega_{Mie} = \sqrt{\hbar^2 N e^2 / mR^2\Delta} = 37 \text{ eV}, \quad (24)$$

in surprisingly good agreement with the experimentally fitted peak positions. This is, however, a coincidence, since the volume plasmon obtained with the monopole operator cannot couple to the electric dipole field. Coupling M dipole operators of the basis set (17) with $L = 1$ and $p = 1, 2, \dots, M$, we obtain the following results for the ingredients of the characteristic equation (8):

$$B_{pp'} = \frac{\hbar^2}{m} \frac{N R^{p+p'-2}}{6} (pp' + 2), \quad (25)$$

$$C_{pp'} = \left(\frac{\hbar^2}{m}\right)^2 \frac{N^2 e^2 R^{p+p'-5}}{3} \left\{ \frac{R}{2\Delta} pp' + \frac{1}{6} (4 - p - p' - 2pp') \right\}. \quad (26)$$

The equation (8) can then again be solved analytically at leading orders in Δ/R ; the calculation is similar to that given in the appendix. The resulting spectrum consists of one surface plasmon at $\hbar\omega_{surf} \simeq 19.8$ eV and $M - 1$ degenerate volume plasmons at $\hbar\omega_{vol} \simeq 31.3$ eV. Thus, the coupling of translational and compressional dipole modes is seen to shift both peaks towards lower energies, the volume peak by a larger amount than the surface peak.

To be more realistic, we now use the quantum-mechanical KS ground-state density $\rho_e(r)$ of Ref.²⁸, include the kinetic energy using the ETF functional $\tau_{ETF}[\rho]$ (up to 4th order, cf. Ref.²¹), and the xc energy in the LDA. The numerical solutions for the LCA spectrum then converge for $M \geq 8$ coupled modes. This is shown in Fig. 4, where the sum-rule weighted LCA spectrum has been Lorentzian folded with a width of $\Gamma = 5$ eV to simulate continuum effects (which were included in the TDLDA calculation). Since the jellium model neglects the ionic structure, the

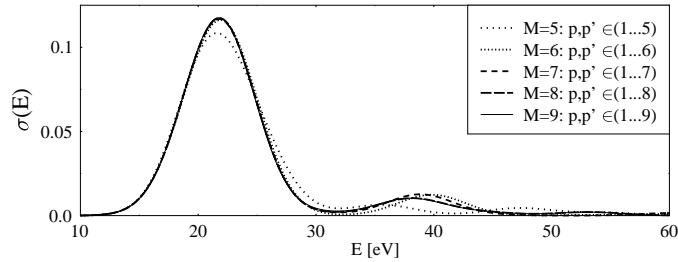


Fig. 4. Convergence of the sum-rule weighted dipole response of C_{60} molecules in the LCA approximation with respect to the number M of coupled modes with $p, p' = 1, \dots, M$. The curves for $M = 8$ (long-dashed) and $M = 9$ (solid) cannot be distinguished (see text for more details).

collective peaks in both the TDLDA and the LCA calculations appear at too low energies, as is known to happen also for metal clusters.¹⁰ Therefore, the TDLDA curve has been artificially blue shifted by 5.5 eV in Ref.¹⁵; we have done the same with our LCA curves. The converged result for $M = 8$ corresponds to the dashed curve in Fig. 3 above. We note that the LCA volume peak now is located at 38 eV, exactly like that of the experimental two-Lorentzian fit.

To account for fragmentation channels that were not measured, the results of the TDLDA calculations were rescaled¹⁵ to fit the height of the experimental surface peak; we do the same here with our LDA results in Fig. 3. We see that both theories underestimate the dipole strength in the high-energy region including the volume peak, but give at least a correct qualitative result. The LCA result, through the explicit use of operators (17) with $p > 1$, confirms the nature of the volume peak as due to compressional components of the collective electronic motion.

Concerning the difference between the two theoretical results, for which the same jellium model was used, we note that in the TDLDA calculation,^{15,28} both $\sigma(n = 1)$ and $\pi(n = 2)$ type valence electrons have explicitly been included in

the microscopic calculation of the linear response; the σ electrons were found to contribute most dominantly in the volume peak region. In our LCA calculation we have, however, used only one type of valence electrons, which might explain the difference of the results particularly in the region of the volume peak.

4. Summary and Outlook

We have briefly reviewed the local current approximation (LCA), a semiclassical approach which can be based on a general variational principle on the same footing as the RPA. In the LCA, the ground state of a finite fermion system is obtained in the selfconsistent mean-field approximation and the collective excitations are described by coupled local operators creating the local currents of the collective motion. This approach, which had earlier been successfully used for collective excitations in nuclei and metal clusters, has here been applied to the optical response of C_{60} molecules. In recent experiments, a volume plasmon has been identified in the photoionization cross section at an energy $\sim 38 \pm 2$ eV, whereas the dominating surface plasmon, already earlier known, was located at $\sim 22 \pm 0.1$ eV. TDLDA calculations reproduce this result qualitatively after applying an *ad hoc* blue shift to compensate for the missing ionic structure in the spherical jellium model used. With the LCA we obtain very similar results as the TDLDA, using the same jellium model and applying the same blue shift, and further using a Lorentzian folding to simulate continuum effects. Since, by explicit construction of the coupled local excitation operators, the collective currents are known in the LCA, we can identify the nature of the volume plasmon in C_{60} as due to compressional components of the collective electronic motion with respect to the ions.

It would be worth while to corroborate our semiclassical interpretation by determining the transition currents both experimentally and theoretically in microscopic TDLDA calculations. Further improvement of the theoretical description should include the ionic structure of the C_{60} molecules. While this might be too time consuming with purely microscopic methods, the LCA appears to be an ideal economic tool for this because the semiclassical nature of the collective electronic currents is little affected by the ionic structure, as known from the corresponding results in metal clusters.

Acknowledgements

We are grateful to M. E. Madjet, R. A. Phaneuf, J. M. Rost and U. Saalman for helpful comments and for providing us with their data used in Fig. 3. One of us (M. B.) acknowledges the hospitality of the Physics Department, University of Nevada at Reno (UNR), during a sabbatical visit, and thanks S. Kümmel and P. G. Reinhard for clarifying discussions.

Appendix: Coupling of surface and volume plasmons in jellium spheres

Here we give a proof of the general solution of the characteristic equation (8) surmised in Ref.¹² for the classical limit with $\rho_e(r) = -\rho_I(r)$ and neglecting kinetic and xc energies. We use the set of operators $Q_p(r) = r^p Y_{L0}(\theta)$ with integer $p = 1, 2, \dots, M$. The equation then becomes, for fixed angular momentum L ,

$$\det |C_{pp'} - (\hbar\omega)^2 B_{pp'}| = f(L) \det |A_{pp'}| = 0, \quad (p, p' = 1, 2, \dots, M) \quad (27)$$

where $f(L)$ is a factor independent of p, p' , and the matrix $A_{pp'}$ is given by

$$A_{pp'} = \frac{(2L+1)pp' + L(L+1)(2L-p-p') - \lambda(2L+1)[pp' + L(L+1)]}{(1+p+p')}, \quad (28)$$

and the eigenvalue λ is the squared ratio of frequencies:

$$\lambda = (\omega/\omega_{vol})^2. \quad (29)$$

We can rewrite the matrix (28) in the following form:

$$A_{pp'} = \frac{(2L+1)[pp' + L(L+1)](1-\lambda) - L(L+1)(1+p+p')}{(1+p+p')}. \quad (30)$$

Now take out a factor $(2L+1)$ from all rows to rewrite (27) as

$$\det |A_{pp'}| = (2L+1)^M \det |D_{pp'}| = 0, \quad (31)$$

where the matrix $D_{pp'}$ is given by

$$D_{pp'} = (1-\lambda)(pp' + F)/(1+p+p') - G, \quad (32)$$

and the constants independent of p, p' are defined as

$$F = L(L+1), \quad G = L(L+1)/(2L+1). \quad (33)$$

We now consider two cases:

a) $L = 0$: Then $F = G = 0$, and the characteristic equation becomes

$$\det |(1-\lambda)pp'/(1+p+p')| = (1-\lambda)^M \det |pp'/(1+p+p')| = 0. \quad (34)$$

Since for any $p, p' > 0$ the determinant on the r.h.s. above is never zero, we get M degenerate solutions with eigenvalue $\lambda = 1$, i.e. with the volume (or bulk) plasma frequency $\omega = \omega_{vol}$ given in (21).

b) $L > 0$: In this case F and G are non-zero and the matrix $D_{pp'}$ has the form

$$D_{pp'} = \begin{pmatrix} (1-\lambda)(1+F)/3 - G & (1-\lambda)(2+F)/4 - G & \dots \\ (1-\lambda)(2+F)/4 - G & (1-\lambda)(4+F)/5 - G & \dots \\ (1-\lambda)(3+F)/5 - G & (1-\lambda)(6+F)/6 - G & \dots \\ \dots & \dots & \dots \end{pmatrix}. \quad (35)$$

Notice that in each element, the first term contains the factor $(1-\lambda)$ and the second term is the constant $-G$. We now replace the first row by the difference between the first and second rows, the second by the difference between the second and third,

12 *Brack, Winkler and Murthy*

and so on, until we reach the last row in which we do not change anything. The determinant, whose value is not altered by these manipulations, then becomes:

$$\det |D_{pp'}| = \begin{vmatrix} (1-\lambda)E_{11} & (1-\lambda)E_{12} & \dots & (1-\lambda)E_{1M} \\ (1-\lambda)E_{21} & (1-\lambda)E_{22} & \dots & (1-\lambda)E_{2M} \\ \dots & \dots & \dots & \dots \\ (1-\lambda)E_{M1} - G & (1-\lambda)E_{M2} - G & \dots & (1-\lambda)E_{MM} - G \end{vmatrix}, \quad (36)$$

where the $E_{pp'}$ are linear expressions in the constant F . Only the in the last row,

the additive constant $-G$ remains, while all other elements now are proportional to $(1 - \lambda)$. The characteristic equation therefore becomes

$$\det |D_{pp'}| = (1 - \lambda)^{(M-1)} \det |\tilde{E}_{pp'}| = 0, \quad (37)$$

where $\tilde{E}_{pp'}$ is the remaining matrix after removing the factor $(1 - \lambda)$ from the first $M - 1$ rows in (36); its determinant is linear in λ . We thus get $M - 1$ degenerate volume plasmons with eigenvalue $\lambda = 1$, i.e. with $\omega = \omega_{vol}$ again. The last eigenvalue is difficult to find in general. But when any one of the p values equals L , the last eigenvalue is found to be $\lambda = LG/F = L/(2L + 1)$, corresponding to the Mie plasmon with angular momentum L , i.e., $\omega_L = \sqrt{L/(2L + 1)}\omega_{vol}$ (cf. Ref.¹²). The generalization of this proof to a set of M arbitrary real values of p is straightforward. For the dipole case $L = 1$ one gets the result stated in the paragraph above (20).

References

1. M. Goldhaber and E. Teller, Phys. Rev. **74**, 1046 (1948).
2. H. von Steinwedel and J. H. D. Jensen, Z. Naturf. Teil A **5**, 413 (1950).
3. A. B. Migdal, J. Phys. USSR **8**, 331 (1944).
4. W. D. Myers *et al.*, Phys. Rev. C **15**, 2032 (1977);
J. Meyer, P. Quentin, B. K. Jennings, Nucl. Phys. A **385**, 269 (1982).
5. P. Gleissl, M. Brack, J. Meyer, P. Quentin, Ann. Phys. (N.Y.) **197**, 205 (1990).
6. see, e.g., the review by B. K. Jennings and A. D. Jackson, Phys. Rep. **66**, 141 (1980).
7. O. Bohigas, A. M. Lane, J. Martorell, Phys. Rep. **51**, 267 (1979).
8. see, e.g., D. J. Rowe: *Nuclear collective motion* (Methuen, London, 1970).
9. G. F. Bertsch and W. Ekardt, Phys. Rev. B **32**, 7659 (1985).
10. M. Brack, Rev. Mod. Phys. **65**, 677 (1993).
11. W. A. de Heer, Rev. Mod. Phys. **65**, 611 (1993),
12. M. Brack, Phys. Rev. B **39**, 3533 (1989).
13. P.-G. Reinhard, M. Brack, O. Genzken, Phys. Rev. A **41**, 5568 (1990);
P.-G. Reinhard and Y. Gambhir, Ann. Phys. (Leipzig) **1**, 598 (1992).
14. S. Kümmel, M. Brack, P.G. Reinhard, Phys. Rev. B **58**, R1774 (1998).
15. S. W. J. Scully *et al.*, Phys. Rev. Lett. **94**, 065503 (2005).
16. G. F. Bertsch, A. Bulgac, D. Tománek, Y. Wang, Phys. Rev. Lett. **67**, 2690 (1991).
17. I. V. Hertel *et al.*, Phys. Rev. Lett. **68**, 784 (1992).
18. S. Kümmel and M. Brack, Phys. Rev. A **64**, 022506 (2001).
19. D. J. Thouless, Nucl. Phys. A **22**, 78 (1961).
20. G. Vignale and W. Kohn, Phys. Rev. Lett. **77**, 2037 (1996);
G. Vignale, C. A. Ullrich, S. Conti, Phys. Rev. Lett. **79**, 4878 (1997).
21. M. Brack and R. K. Bhaduri: *Semiclassical Physics*, Frontiers in Physics, Vol. 96 (revised edition: Westview Press, Boulder, 2003); see Ch. 4 for the ETF model.
22. E. Lipparini and S. Stringari, Phys. Rep. **175**, 103 (1989).
23. W. Ekardt, Phys. Rev. B **29**, 1558 (1984).
24. M. Schmidt and H. Haberland, Eur. Phys. J. D **6**, 109 (1999).
25. B. Montag and P.-G. Reinhard, Z. Phys. D **33**, 265 (1995).
26. W. Knight *et al.*, Phys. Rev. Lett. **52**, 2141 (1984).
27. M. J. Puska and R. M. Nieminen, Phys. Rev. A **47**, 1181 (1993).
28. A. Rüdél *et al.*, Phys. Rev. Lett. **89**, 125503 (2002).
29. A. V. Korol and A. V. Solov'yov, Phys. Rev. Lett. **98**, 179601 (2007).
30. S. W. J. Scully *et al.*, Phys. Rev. Lett. **89**, 179602 (2007).